Chromaticity of the Martian sky as observed by the Mars Exploration Rover Pancam instruments

Article *in* Journal of Geophysical Research Atmospheres · September 2006

DOI: 10.1029/2006JE002687

Dmitry Savransky
Cornell University

M. J. Wolff
The Space Science Institute

JOURNAL OF GEOPHYSICAL RESEARCH, VOL. 111, E12S05, doi:10.1029/2006JE002687, 2006

Click Here for Full Article

Chromaticity of the Martian sky as observed by the Mars Exploration Rover Pancam instruments

J. F. Bell III,[1] D. Savransky,[1] and Michael J. Wolff[2]

Received 26 January 2006; revised 23 March 2006; accepted 3 April 2006; published 28 September 2006.

[1] We have derived quantitative color estimates of the Martian sky from data acquired by the Panoramic Cameras (Pancams) on the Mars Exploration Rovers Spirit and Opportunity. We calculate the perceptual color of the sky directly from the absolute radiometric calibration of the cameras, following similar approaches to those used in previous studies with Viking Lander and Mars Pathfinder data. We further use these measurements to study changes in sky color throughout the MER missions and to compare these to changes in atmospheric opacity determined from direct solar imaging by the Pancams. We have derived a functional relationship between sky color and optical depth and discuss its possible uses and limitations. Finally, we simulate changes in sky color as suspended dust is removed and present visual representations of these based on modeling results, past studies, and observed MER sky brightnesses. The color of the Martian sky as opacity decreases from 1.0 to 0.0 is estimated to change from "dark yellowish brown" at high opacity to "bluish-black" or "black" if dust-free.

Citation: Bell, J. F., III, D. Savransky, and M. J. Wolff (2006), Chromaticity of the Martian sky as observed by the Mars Exploration Rover Pancam instruments, *J. Geophys. Res.*, *111*, E12S05, doi:10.1029/2006JE002687.

1. Introduction

[2] The Mars Exploration Rover (MER) missions of Spirit and Opportunity have now each spent over a full Martian year traversing and performing scientific observations in Gusev crater and Meridiani Planum [e.g., *Arvidson et al.*, 2006; S. W. Squyres et al., Overview of the Opportunity Mars Exploration Rover Mission to Meridiani Planum: Eagle Crater to Purgatory Ripple, submitted to *Journal of Geophysical Research*, 2006]. The long durations of these missions provide us with the opportunity to study atmospheric changes on diurnal to seasonal timescales and to compare them to long-term observations acquired from telescopic, orbiter, and Viking Lander instruments [e.g., *Pollack et al.*, 1979; *Arvidson et al.*, 1989a; *Martin et al.*, 1992; *Clancy et al.*, 1995; *Wolff et al.*, 1997]. Although the rovers were primarily designed for geological science activities, several of the instruments are regularly involved in atmospheric studies. The Pancams, in particular, are valuable tools in studying the Martian sky due to their multispectral and high resolution imaging capabilities [*Bell et al.*, 2003, 2004a, 2004b; *Lemmon et al.*, 2004; M. T. Lemmon et al., The visible optical depth record of the Mars Exploration Rovers first Mars year, submitted to *Journal of Geophysical Research*, 2006 (hereinafter referred to as Lemmon et al., submitted manuscript, 2006)].

[3] Several sets of Pancam atmospheric observations have been conducted systematically over the course of both MER missions. These include determination of the visible wavelength optical depth using daily (or more frequent) direct observations of the Sun with the Pancam solar filters [e.g., *Bell et al.*, 2003; *Lemmon et al.*, 2004], and multispectral imaging of the sky (Lemmon et al., submitted manuscript, 2006). One component of the sky imaging campaign has been a systematic set of observations of the horizon in a particular direction and at a particular time of sol (a Martian day), for many sols in a row. These latter observations are called Horizon Surveys and they allow us to characterize the sky color, its diurnal variations, and its dependence on the atmospheric dust loading.

[4] In this paper, we describe the Horizon Survey campaigns conducted on both Spirit and Opportunity during their first Mars year of operations, and how these kinds of data can be used to derive the quantitative color of the Martian sky and to infer information on the overall atmospheric dust opacity and the multispectral and scattering properties of the dust itself. First we review the observations and some of the concepts of quantitative colorimetry as they apply to the MER data sets, and then we describe the method by which calibrated radiance data from the Horizon Surveys are converted into quantitative sky chromaticity estimates. We then present results for the derived sky chromaticities during the course of both missions, and compare these values to the optical depths derived from direct solar imaging. Not surprisingly, a strong correlation is found between sky color and dust opacity, allowing the former to be used as an accurate predictor of the latter in cases where a direct determination of opacity does not exist or cannot be obtained for instrumental or operational reasons. Finally, we provide some calculations and speculations on the nature of the Martian sky color during

[1]Department of Astronomy, Cornell University, Ithaca, New York, USA.

[2]Space Science Institute, Boulder, Colorado, USA.

0148-0227/06/2006JE002687$09.00

Table 1. Spirit Horizon Survey Sequences[a]

Sol	Seq	L_s	LTST	tau	*x*	*y*
391	P2664	156.612	12:37:55	0.831	0.404	0.376
392	P2664	157.147	12:38:04	1.020	0.408	0.378
393	P2664	157.687	12:38:13	0.905	0.406	0.377
394	P2664	158.254	12:38:22	0.854	0.406	0.377
399	P2664	160.941	12:37:21	0.862	0.405	0.377
400	P2664	161.489	12:43:33	0.904	0.405	0.377
401	P2664	162.052	12:40:22	0.885	0.405	0.377
402	P2664	162.634	12:39:29	0.945	0.406	0.377
403	P2664	163.147	12:39:32	0.885	0.405	0.377
405	P2664	164.262	12:40:06	0.820	0.404	0.377
406	P2664	164.827	12:40:59	0.801	0.405	0.377
407	P2664	165.384	13:27:15	0.723	0.398	0.375
408	P2664	165.891	12:47:52	0.771	0.403	0.376
410	P2664	167.038	12:42:31	0.691	0.402	0.376
412	P2664	168.156	12:42:45	0.664	0.402	0.376
414	P2664	169.260	12:37:58	0.689	0.402	0.376
415	P2664	169.817	12:43:04	0.767	0.403	0.376
427	P2664	176.635	12:46:46	0.727	0.401	0.376
429	P2664	177.748	12:19:20	0.754	0.404	0.376
430	P2664	178.325	12:42:23	0.702	0.401	0.376
431	P2664	178.929	12:42:26	0.672	0.401	0.375
433	P2664	180.088	12:42:44	0.672	0.400	0.375
434	P2664	180.661	12:42:47	0.728	0.400	0.375
435	P2664	181.232	12:42:50	0.701	0.401	0.375
436	P2664	181.844	13:03:43	0.671	0.399	0.375
462	P2664	197.258	10:34:40	0.626	0.404	0.377
464	P2664	198.513	12:33:41	0.643	0.399	0.375
465	P2664	199.096	12:51:30	0.618	0.397	0.374
466	P2664	199.736	12:51:55	0.731	0.398	0.375
467	P2664	200.323	12:02:33	0.630	0.401	0.376
468	P2681	200.949	12:50:18	0.568	0.398	0.375
469	P2681	201.581	12:52:30	0.603	0.399	0.375
470	P2681	202.207	18:34:27	0.613	0.362	0.360
480	P2681	208.417	18:34:40	0.630	0.355	0.356
489	P2681	214.004	12:48:07	0.697	0.399	0.375
492	P2681	215.839	12:37:52	0.765	0.402	0.376
501	P2681	221.603	12:39:57	1.017	0.406	0.377
504	P2681	223.536	12:51:08	1.171	0.406	0.378
515	P2629	230.619	11:39:01	1.358	0.416	0.381
516	P2629	231.183	11:38:27	1.281	0.415	0.381
517	P2629	231.818	11:13:03	1.184	0.415	0.381
519	P2629	233.187	11:37:04	1.179	0.413	0.380
520	P2629	233.838	11:36:19	1.183	0.412	0.380
521	P2629	234.441	11:25:51	1.240	0.414	0.380
523	P2629	235.801	11:34:48	1.228	0.414	0.380
524	P2629	236.427	11:34:17	1.245	0.413	0.380
525	P2629	237.031	11:36:29	1.236	0.413	0.380
526	P2629	237.722	11:33:14	1.250	0.413	0.380
527	P2629	238.371	11:32:45	1.207	0.412	0.380
528	P2629	238.985	11:32:23	1.190	0.413	0.380
529	P2629	239.650	11:31:40	1.175	0.413	0.380
530	P2629	240.319	11:32:32	1.173	0.412	0.380
532	P2629	241.601	11:36:22	1.146	0.412	0.380
533	P2629	242.263	11:30:58	1.160	0.413	0.380
534	P2629	242.915	11:28:37	1.153	0.413	0.380
535	P2629	243.555	11:32:59	1.132	0.412	0.380
536	P2629	244.226	11:27:23	1.167	0.413	0.380
537	P2629	244.888	11:26:57	1.169	0.412	0.380
538	P2629	245.514	11:16:20	1.130	0.412	0.380
543	P2629	248.793	11:22:59	1.118	0.411	0.380
544	P2629	249.445	11:22:20	1.082	0.411	0.380
545	P2629	250.099	11:11:47	1.063	0.411	0.380
546	P2629	250.727	11:20:58	1.094	0.411	0.379
547	P2629	251.416	11:30:30	1.069	0.410	0.379
606	P2629	289.435	11:46:16	0.728	0.401	0.376
608	P2629	290.651	12:59:49	0.661	0.395	0.374
610	P2629	291.920	12:44:21	0.683	0.396	0.374
611	P2629	292.487	12:51:39	0.670	0.396	0.374
613	P2629	293.771	12:33:35	0.682	0.398	0.374
656	P2629	319.783	14:29:50	0.785	0.402	0.375

Notes to Table 1:

[a]Sol is the rover specific sol, Seq is the sequence name, L_s is the aerocentric longitude of the Sun, LTST refers to the local true solar time, tau is the optical depth as measured by the L8 filter, and *x* and *y* are the average chromaticities from pixels 20 through 1000 by 512 through 1000 of the horizon surveys, using equations (1) through (3).

extremely high dust and low dust conditions, both of which are scenarios that provide important bounds on the radiative and scattering behavior of the atmosphere as a whole.

2. Observations

[5] Many MER/Pancam observation sequences have been devoted to atmosphere and Sun imaging. Most of these are conducted as long-term systematic campaigns designed to monitor the visible-wavelength dust opacity [e.g., *Lemmon et al.*, 2004] or to characterize the scattering properties of atmospheric dust at a variety of solar phase angles (e.g., Lemmon et al., submitted manuscript, 2006). Additional special atmospheric sequences are often conducted to search for water ice clouds, dust devils, or to characterize the vertical distribution of aerosols during twilight, sunrise, and sunset imaging. One set of systematic observations that has been run intermittently for many sols in a row on both rovers is known as the "Horizon Survey." This observation acquires 3 full frame (1024 × 1024 pixel) images using filters L4, L5 and L6 (601, 535 and 482 nm), pointed 3° above the horizon and directly to the west (this ensures that the majority of the image will be taken up by the sky, that the image will include the horizon, and that the Sun will not be captured). The observation is acquired in the morning or early afternoon, typically within half an hour of 11:30 or 12:30 Local True Solar Time (LTST) for Spirit (Table 1) and 11:45 LTST for Opportunity (Table 2).

3. CIE Colorimetry

[6] The idea that the human eye contains receptors sensitive to three specific colors first originated in the 19th century, and immediately led to attempts to define all colors in terms of three primaries. However, James Clerk Maxwell demonstrated that no additive combination of three primary colors (any set of colors which, when added in appropriate amounts produce white) could cover the entire gamut of colors perceived by the eye. He was also the first to show that the set of primaries is not unique, and can be made up of many combinations of three colors. During the 1920s, experiments with the Red, Green and Blue primaries showed that the entire range of spectral colors could be defined quantitatively using tristimulus values (the amounts of each primary present in the color), only if negative values were allowed for the red tristimulus value [*Wyszecki and Stiles*, 1982].

[7] In 1931 the Commission International de l'Eclairage (CIE) created a standardized system of quantitative color measurement in which all tristimulus values would be positive [*CIE*, 1932]. This color space was defined in terms of chromaticity coordinates; the tristimulus values scaled by their sum, which reflect a color's hue and saturation, but not its absolute brightness. Since the CIE chromaticities for a given color add to 1, it is possible to define any color using only two coordinates (x and y) and to map the visible colors

Table 2. Opportunity Horizon Survey Sequences[a]

Sol	Seq	L_s	LTST	tau	*x*	*y*
360	P2663	151.052	11:48:35	0.891	0.397	0.380
361	P2663	151.564	11:48:44	0.956	0.397	0.380
362	P2663	152.119	11:48:53	0.922	0.397	0.380
363	P2663	152.646	11:48:41	0.897	0.397	0.380
364	P2663	153.119	11:48:46	0.937	0.397	0.380
366	P2663	154.209	11:49:09	0.892	0.397	0.380
367	P2663	154.705	11:49:27	0.919	0.397	0.380
369	P2663	155.816	12:00:19	0.931	0.396	0.380
370	P2663	156.375	11:15:28	0.875	0.398	0.381
371	P2663	156.901	11:59:59	0.889	0.396	0.380
372	P2663	157.425	11:50:52	0.931	0.397	0.380
373	P2663	157.986	11:35:26	0.926	0.397	0.380
374	P2663	158.489	10:05:02	0.959	0.401	0.382
379	P2663	161.243	11:51:25	0.860	0.397	0.380
380	P2663	161.776	11:51:15	0.808	0.396	0.380
381	P2663	162.325	11:11:21	0.771	0.397	0.380
382	P2663	162.870	11:51:52	0.783	0.396	0.380
399	P2663	172.339	11:53:37	0.788	0.396	0.380
400	P2663	172.925	11:53:47	0.767	0.396	0.380
401	P2663	173.467	11:53:48	0.792	0.396	0.380
402	P2663	174.048	11:54:04	0.762	0.396	0.380
403	P2663	174.609	11:53:59	0.750	0.395	0.380
404	P2663	175.175	11:54:21	0.770	0.396	0.380
405	P2663	175.746	11:30:13	0.780	0.398	0.381
408	P2663	177.501	12:14:50	0.785	0.395	0.380
409	P2663	178.047	11:58:43	0.777	0.396	0.380
413	P2663	180.376	11:55:47	0.776	0.396	0.380
414	P2663	180.975	11:55:01	0.780	0.396	0.380
417	P2663	182.666	11:57:15	0.786	0.396	0.380
419	P2663	183.852	11:57:38	0.817	0.397	0.380
421	P2663	185.039	12:00:18	0.806	0.396	0.380
422	P2663	185.610	11:57:40	0.849	0.397	0.380
423	P2663	186.214	11:55:20	0.832	0.397	0.380
424	P2663	186.780	11:55:58	0.886	0.398	0.381
426	P2663	188.005	11:55:55	0.870	0.398	0.381
427	P2663	188.559	11:25:57	0.834	0.399	0.381
428	P2663	189.164	11:25:19	0.856	0.399	0.381
429	P2663	189.748	11:27:43	0.880	0.398	0.381
430	P2663	190.327	11:26:06	0.916	0.400	0.381
437	P2663	194.576	12:00:33	0.941	0.399	0.381
438	P2663	195.156	12:00:31	0.832	0.397	0.380
440	P2663	196.353	12:42:05	0.856	0.393	0.379
443	P2663	198.161	11:54:49	0.818	0.396	0.380
444	P2663	198.744	11:54:32	0.846	0.396	0.380
445	P2663	199.376	11:54:25	0.826	0.396	0.380
446	P2663	200.001	11:54:20	0.813	0.396	0.380
447	P2679	200.633	11:43:39	0.731	0.396	0.380
453	P2679	204.348	11:53:41	0.724	0.395	0.380
456	P2679	206.195	10:37:58	1.145	0.403	0.382
464	P2679	211.167	12:31:39	0.854	0.396	0.380
475	P2679	218.117	11:58:25	0.862	0.397	0.381
476	P2679	218.748	11:48:03	0.980	0.399	0.381
477	P2679	219.383	11:47:42	0.977	0.400	0.381
478	P2679	220.001	11:47:21	0.924	0.399	0.381
479	P2679	220.664	11:46:50	0.981	0.400	0.382
480	P2679	221.301	11:46:38	1.058	0.401	0.382
481	P2679	221.923	11:47:27	1.137	0.403	0.382
482	P2679	222.578	11:45:55	1.227	0.403	0.383
483	P2679	223.205	11:35:36	1.163	0.404	0.383
484	P2679	223.836	11:45:09	1.220	0.404	0.383
485	P2679	224.431	11:44:49	1.201	0.403	0.383
486	P2679	225.074	11:44:23	1.238	0.405	0.383
487	P2679	225.738	11:43:58	1.272	0.405	0.383
488	P2629	226.401	11:43:36	1.434	0.409	0.384
489	P2629	227.030	11:43:19	1.584	0.411	0.385
490	P2629	227.714	11:42:45	1.643	0.412	0.385
491	P2629	228.317	11:32:18	1.817	0.415	0.386
492	P2629	228.961	11:31:52	1.816	0.414	0.386
494	P2629	230.275	11:30:57	1.522	0.411	0.385
495	P2629	230.893	11:30:59	1.470	0.411	0.385
496	P2629	231.548	11:34:31	1.366	0.409	0.384
497	P2629	232.185	11:38:28	1.285	0.406	0.384
499	P2629	233.478	11:38:30	1.220	0.406	0.383
500	P2629	234.168	11:37:58	1.174	0.406	0.383
502	P2629	235.438	11:27:03	1.207	0.406	0.384
504	P2629	236.721	11:35:50	1.291	0.407	0.384
506	P2629	238.013	11:33:46	1.206	0.406	0.383
507	P2629	238.669	11:34:10	1.199	0.406	0.384
508	P2629	239.296	11:25:19	1.211	0.406	0.384
510	P2629	240.631	11:41:43	1.233	0.406	0.383
511	P2629	241.274	11:31:54	1.229	0.406	0.384
512	P2629	241.967	11:32:59	1.265	0.406	0.384
513	P2629	242.599	11:32:24	1.199	0.406	0.384
514	P2629	243.225	11:31:47	1.184	0.406	0.384
516	P2629	244.555	11:30:37	1.188	0.406	0.383
517	P2629	245.187	11:19:53	1.161	0.406	0.384
523	P2629	249.127	11:24:38	1.168	0.406	0.383
584	P2629	288.427	11:43:30	0.800	0.398	0.381
585	P2629	289.075	11:31:11	0.814	0.399	0.381
586	P2629	289.712	11:52:07	0.787	0.398	0.381
587	P2629	290.316	11:57:11	0.791	0.397	0.380
589	P2629	291.595	10:40:46	0.835	0.399	0.381
590	P2629	292.232	10:40:04	0.778	0.400	0.381
591	P2629	292.835	10:32:18	0.774	0.400	0.381
592	P2629	293.432	10:19:27	0.807	0.400	0.381
593	P2629	294.082	10:05:42	0.765	0.400	0.381
594	P2629	294.710	10:13:27	0.778	0.400	0.381
595	P2629	295.290	10:14:43	0.836	0.400	0.381
596	P2629	295.934	10:13:34	0.758	0.400	0.381
599	P2629	297.789	10:49:50	1.056	0.401	0.382
600	P2629	298.413	11:21:16	0.787	0.398	0.381
601	P2629	299.041	10:45:36	0.788	0.399	0.381
602	P2629	299.638	10:41:30	0.737	0.399	0.381
603	P2629	300.266	10:41:41	0.735	0.399	0.381

[a]Sol is the rover specific sol, Seq is the sequence name, Ls is the aerocentric longitude of the Sun, LTST refers to the local true solar time, tau is the optical depth as measured by the L8 filter and *x* and *y* are the average chromaticities from pixels 20 through 1000 by 512 through 1000 of the horizon surveys, using equations (1) through (3).

onto a two dimensional surface, which is commonly known as the CIE chromaticity diagram. [e.g., *Wyszecki and Stiles*, 1982]. The 1931 CIE definition has become the standard method of defining colors. It allows direct comparison of color data collected by different instruments in different environments, as well as direct mapping of quantitative values to visible colors.

[8] Furthermore, the National Bureau of Standards-Inter-Society Color Council (NBS-ISCC) publishes a standardized set of color names and modifiers that can be used to name colors of specific chromaticity values in a way that is more accessible and understandable than a set of numbers [e.g., *Kelly and Judd*, 1976; *Mundie*, 1995]. Assigning names to colorimetric values, calculated from an absolute radiance calibration, allows us to quote colors that would closely approximate what would be seen by humans present on Mars.

4. Calculating Chromaticities From MER Pancam Data

[9] The method by which calibrated Pancam radiance images can be converted to quantitative chromaticity estimates was initially described by *Bell et al.* [2006]. Here we expand and augment that discussion in more detail. Eight of the fifteen glass interference filters used by the Pancam instruments fall into the human visible portion of the spectrum (380 to 780 nm). Six of these are located on

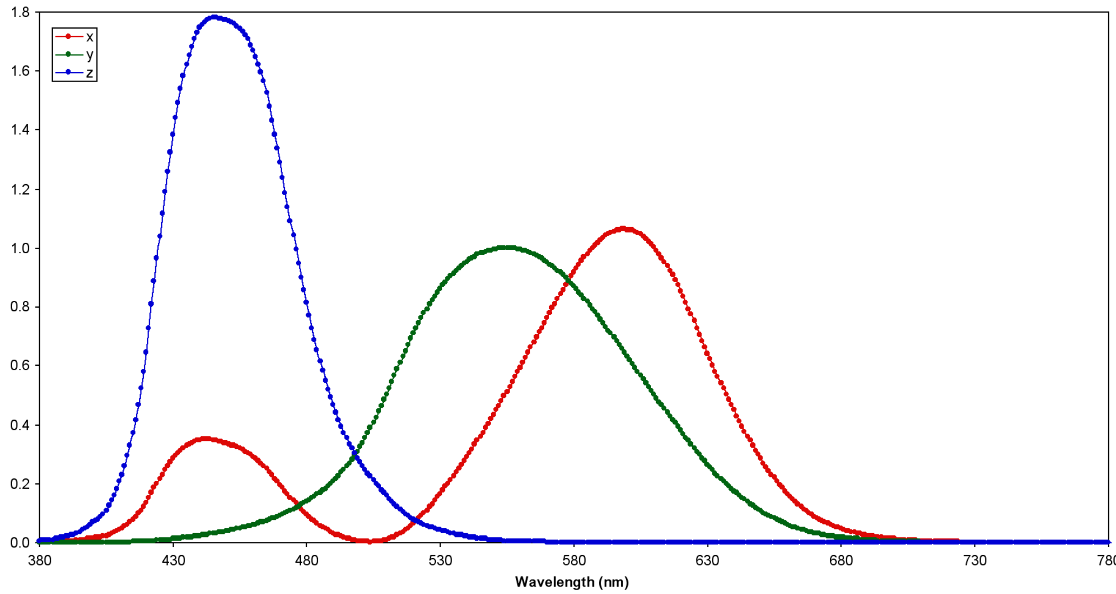

Figure 1. CIE color matching functions [*CIE*, 1932].

the filter wheel on the left camera and are referred to as L2, L3, L4, L5, L6 and L7, corresponding to wavelengths of 753, 673, 601, 535, 482, and 432 nm, respectively [*Bell et al.*, 2003]. The remaining two visible wavelength filters are on the right camera filter wheel (R1 and R2 at 432 and 753 nm, respectively) and provide stereo support for the L2 and L7 filters. Only the left eye filter set is used for deriving chromaticity values as described here.

[10] The raw data transmitted from the rovers is processed via a calibration pipeline to produce images calibrated to radiance (W/m^2/nm/sr) as described by *Bell et al.* [2003, 2006]. These values are taken to be an accurate representation of the spectral power distribution of the imaged scenes and are based on an absolute calibration of the cameras, eliminating the requirement of knowing the exact illumination of the scene.

[11] For an emissive source's Spectral Power Distribution, tristimulus values can be written in the form:

$$X = \frac{1}{N}\sum_{i=\lambda_1}^{\lambda_2} \bar{x}_i P_i$$
$$Y = \frac{1}{N}\sum_{i=\lambda_1}^{\lambda_2} \bar{y}_i P_i \qquad (1)$$
$$Z = \frac{1}{N}\sum_{i=\lambda_1}^{\lambda_2} \bar{z}_i P_i$$

where λ_1 and λ_2 mark the bounds of the human visible spectrum, P_i are the wavelength dependent spectral power distribution values, and $\bar{x}$, $\bar{y}$, $\bar{z}$ are the standard CIE color matching function values (Figure 1). N is a normalizing factor chosen such that y is equal to 1.0 for pure white (sample reflects 100% of all wavelengths). This allows for the Y tristimulus value to correspond with the luminance (brightness) of the object being measured.

[12] As previously stated, chromaticities are calculated by scaling tristimulus values by their sum:

$$x = \frac{X}{(X+Y+Z)}$$
$$y = \frac{Y}{(X+Y+Z)} \qquad (2)$$
$$z = \frac{Z}{(X+Y+Z)}$$

and since $x + y + z = 1$, we need only retain x and y. The scaling factor N is not necessary for the calculation of x and y chromaticity (since it gets factored out in equation (2)), but

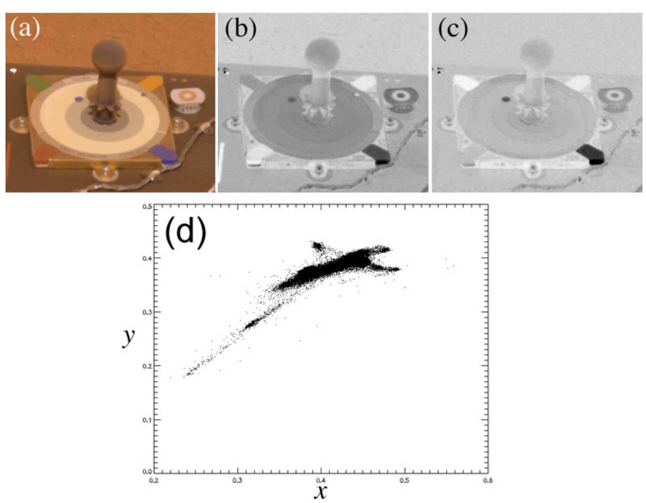

Figure 2. Spirit Pancam calibration target ("MarsDial") image from sequence P2111, Sol 50. (a) True color image [*Bell et al.*, 2006]; (b) x chromaticity image; (c) y chromaticity image; (d) scatterplot of x versus y chromaticities.

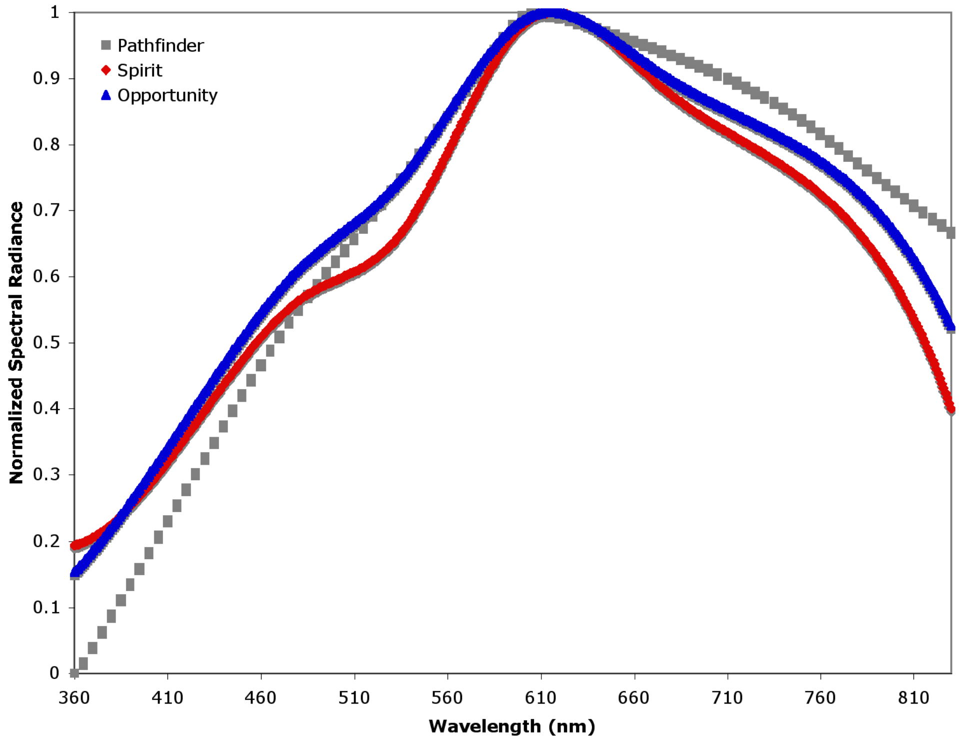

Figure 3. Averaged normalized radiance spectra of the Martian sky. The Spirit spectrum was produced from sky flats taken on sols 120, 280, and 377. The Opportunity spectrum was produced from sky flats taken on sols 4 and 353. See text for details. The Pathfinder spectrum is from *Maki et al.* [1999]. Each spectrum is normalized to its maximum.

is needed if we want to report luminance (Y) values. Thus x, y and Y values can be used to describe all attributes of any color (hue, saturation and brightness) [*Wyszecki and Stiles*, 1982].

[13] Since the Pancams are not able to image pure white sources on Mars, it is necessary to calculate from available pre-flight calibration data the radiance values which the cameras would record if viewing a 100% reflective surface. We have calculated these estimated white radiances using measurements performed at the Bloomsburg University Goniometer (BUG) facility [*Shepard*, 2001], which was used to measure the bidirectional reflectance of the Pancam Calibration Target (caltarget) substrates over a range of geometries prior to launch [*Bell et al.*, 2003].

[14] We interpolate from the BUG data for the white, gray, and black caltarget regions and multiply by a normalization coefficient in order to develop the predicted white region reflectances on Mars. The normalization coefficient is calculated by integrating over all available BUG geometries, and scaling such that the integral agrees with the directional hemispherical reflectance data for the caltarget regions as reported by *Bell et al.* [2003]. We divide spectral data measured from the caltargets on Mars by this calculated spectrum and use the results in equation (1), which allows us to solve for the scaling factor N.

[15] The procedure for calculating Pancam chromaticities is as follows: for each pixel, a cubic spline is fit to the observed radiance values from the six available left camera wavelengths to produce a spectrum from 380 to 780 nm in intervals of one nanometer. This spectrum is multiplied point by point with the 3 CIE color matching function values (Figure 1) and each of the resultant arrays is summed to produce the three tristimulus values. These are then divided by their sum and the x and y chromaticities are retained as two dimensional arrays matching the orientation and pixel placement of the original images. Thus, for each Pancam image to which this process is applied, two chromaticity images are produced, allowing specific areas to be extracted and analyzed on the basis of pixel placement in the original image (Figure 2). As an optional additional step, we retrieve data for the white caltarget region from the calibration pipeline [*Bell et al.*, 2003, 2006] for the caltarget closest in time to the image being processed, and calculate the scaling factor N as described above to produce a third array of Y values.

5. Calculation of Chromaticities From Incomplete Filter Sets

[16] Because of operational limitations on the rovers with regards to onboard storage capacity and available daily power or downlink data volume, it is standard practice to make observations as small as possible while still gathering the data needed for the observation's scientific purpose. To this end, most systematic observations do not employ all thirteen of the multispectral "geology" filters, nor even all of the six left eye filters listed above. Although the procedure for calculating chromaticity values can be applied to any subset of filters, using a limited filter set produces poorer results. Images made directly from only two or three filters differ greatly from those made from the full six filter set in terms of spectra and chromaticity values. Also the

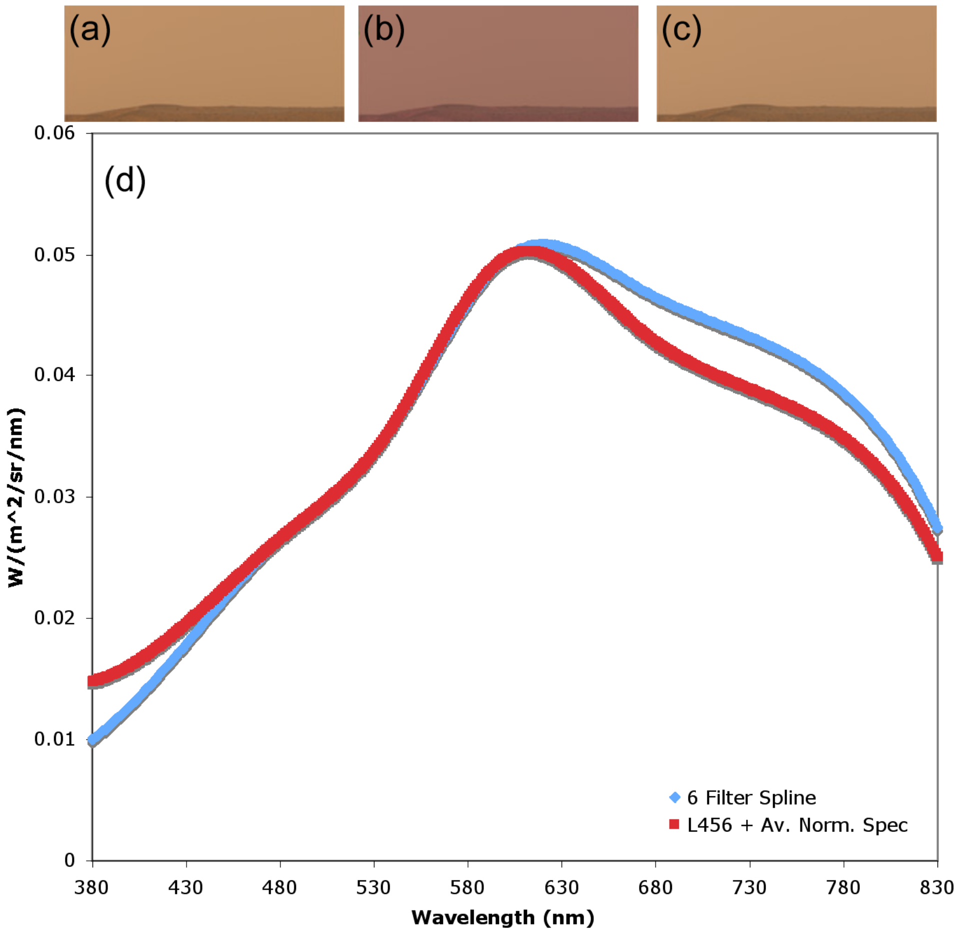

Figure 4. Color composite images from Opportunity sol 3 (sequence P2350). (a) True color rendering [*Bell et al.*, 2006] using all six visible spectrum filters. (b) Color rendering using only L4, L5, and L6. (c) Color rendering using L4, L5, L6, and the average normalized sky spectrum with equation (3). (d) Averaged splined spectrum using all six filters (blue), and spectrum produced from three filters and the average normalized sky spectrum (red).

images differ significantly in color, which can be used as a guide to chromatic accuracy by those with long experience with ground-based visual observation of Mars. In order to obtain the most accurate estimates of chromaticities from these spectrally subsampled images, it is necessary to synthesize a more complete spectral profile by using the available values from the image and an average normalized spectrum for different scene materials. For this study, an average normalized sky spectrum was created for each rover by averaging "sky flat" observations [*Bell et al.*, 2006] from throughout the mission. As can be seen from Figure 3, despite being on opposite sides of the planet, the shapes of the average sky spectra seen by the rovers are very similar.

[17] When processing images that are missing some filter information, approximate values for the missing filters are calculated by summing the existing wavelength information scaled to the missing wavelength using the average normalized spectrum, and weighted by their difference in wavelength:

$$P_m = \sum_{i=\lambda_1}^{\lambda_n} \left(P_i \frac{S_m}{S_i} \right) \left(\frac{1}{|\lambda_m - \lambda_i|} \right) \quad (3)$$

where P_m and S_m are the spectral power at the missing wavelength and the value of the average normalized spectrum at the missing wavelength, respectively, and λ_1 through λ_n are the wavelengths of the filters whose spectral values are known. This method can be used to produce much more accurate results for images taken with a subset of the left eye filters, as can be seen in Figure 4.

[18] We can check the accuracy of this method as applied to the horizon surveys by comparing the chromaticities calculated for a 3-filter Horizon Survey to those calculated from an image of the sky taken in all six visible spectrum filters at the same time of day. Although large portions of the sky are not often imaged using all six of the human visible wavelength filters, there are enough examples to perform this comparison. Another systematic MER atmospheric imaging sequence, the Sky Survey, is very useful in this respect. This sequence begins with a measure of optical depth with both Pancam solar filters (pointing at the Sun) and continues by imaging multiple portions of the sky with all 13 remaining narrowband filters. Unfortunately, the lowest pointing in this sequence is centered at 17°, placing it closer to the Sun than the portion of the sky imaged by the Horizon Surveys. Also, unlike the Horizon Surveys, the time of day when the Sky Survey sequences are run changes frequently. Despite this,

Table 3. Spirit Sky Survey Sequences (P2619)[a]

Sol	LTST	*x*	*y*	% *x* Diff	% *y* Diff
393	13:37:00	0.411	0.382	1.135	6.268
405	14:37:24	0.411	0.382	1.554	5.739
426	14:34:27	0.410	0.383	2.028	4.935
428	12:47:29	0.408	0.382	1.586	5.210
429	12:02:40	0.404	0.380	0.231	6.323
430	11:43:17	0.402	0.378	0.147	6.119
431	13:37:03	0.410	0.382	2.163	4.866
432	14:59:27	0.409	0.382	1.946	4.886
433	11:36:58	0.400	0.377	0.077	6.129
433	13:33:35	0.409	0.382	2.059	4.817
433	16:06:35	0.404	0.380	0.855	5.275
434	12:06:26	0.403	0.379	0.673	5.667
434	13:58:31	0.409	0.382	2.077	4.876
435	12:00:16	0.403	0.378	0.495	5.843
435	13:47:59	0.409	0.382	2.029	4.891
437	15:31:00	0.406	0.381	1.818	4.592
444	16:27:39	0.398	0.378	0.208	5.431
445	14:02:58	0.407	0.382	2.107	4.409
456	12:20:49	0.404	0.380	0.103	6.388
479	12:45:01	0.405	0.381	6.327	6.815
486	12:42:15	0.405	0.381	1.488	4.824
493	12:39:46	0.408	0.382	1.535	5.163
512	11:23:48	0.420	0.386	0.804	6.683
519	12:29:49	0.417	0.386	0.980	6.978
526	12:26:01	0.417	0.386	0.898	6.087
545	12:22:13	0.415	0.385	0.859	6.883
558	13:19:36	0.414	0.385	1.054	6.501

[a]Sol is the rover specific sol, LTST refers to the local true solar time, and x and y are the average chromaticities of the Sky Surveys. The chromaticity percent differences are calculated using the closest available Horizon Survey chromaticity values (by sol and time of day).

we find that the chromaticities calculated from the full-spectrum Sky Survey sequences consistently differ by less than 7% from chromaticities derived from Horizon Surveys using the method described above (Tables 3 and 4 and Figure 5). There are also a few non-systematic sequences which image the sky using the full set of human visible wavelength filters and which have been run at approximately the same time of day as the Horizon Surveys. For example, on Opportunity sol 357 a sequence was run pointing directly at the sky at local noon using all 13 filters. The chromaticities calculated from this differ from those calculated from the 3 filter Horizon Survey taken at 11:48 LTST on sol 360 by only 1%.

[19] With the ability to calculate chromaticity, and systematic multispectral observations, it is possible to track changes in the sky color. The Horizon Survey observation described above was run on 87 of the 140 sols between sol 360 and 600 on Opportunity, within half an hour of 11:45 LTST. On Spirit, the same observation was run 27 times between sols 515 and 547 centered on 11:30 LTST, and 37 times between sols 391 and 613 centered at 12:30 LTST. There are multiple meaningful ways of displaying these data. Figure 6 shows spatially compressed "panels" created from the radiance calibrated Horizon Survey images, which show distinct changes in sky color over time in a way comparable to the Viking Lander sky color change images presented by *Arvidson et al.* [1983] and posted online at http://www.lpi.usra.edu/publications/slidesets/winds/slide_29.html. Figure 7 shows the chromaticity values plotted as a function of sol and solar longitude.

[20] Because chromaticity is an absolute measure of color, we can compare these results with those derived from measurements by previous missions. The sky chromaticities measured by both Viking lander cameras [*Huck et al.*, 1977] and the Imager for Mars Pathfinder [*Maki et al.*, 1999] are consistent with those measured by the MER rovers (Table 5). The MER data have a slightly higher range than the Pathfinder data, which is perhaps explained by the fact that the data were collected over a much greater time range. All of these values confirm the ISCC-NBS color designations of "light to moderate yellowish brown" for the typical color of the Martian sky.

6. Chromaticity and Optical Depth Measurements

[21] The single most often run Pancam observation on both rovers is direct imaging of the Sun through two filters designed for this purpose: L8 (440 nm) and R8 (880 nm) [*Bell et al.*, 2003; *Lemmon et al.*, 2004; Lemmon et al.,

Table 4. Opportunity Sky Survey Sequences (P2619)[a]

Sol	LTST	*x*	*y*	% *x* Diff	% *y* Diff
361	13:25:43	0.398	0.384	0.065	3.460
373	12:37:12	0.394	0.382	0.747	3.897
382	13:21:55	0.394	0.383	0.415	3.411
425	13:20:52	0.399	0.385	0.302	3.214
435	14:26:11	0.399	0.385	0.184	3.401
443	10:28:00	0.380	0.374	4.158	5.878
444	10:27:57	0.381	0.374	4.119	5.894
445	10:27:49	0.380	0.374	4.186	5.933
446	10:27:52	0.381	0.374	4.049	5.821
449	11:54:50	0.390	0.381	1.448	3.877
452	14:58:32	0.396	0.385	0.370	2.698
454	12:05:07	0.392	0.382	0.828	3.365
455	11:56:53	0.393	0.383	0.504	3.191
457	11:34:38	0.392	0.381	0.852	3.572
458	11:38:14	0.392	0.381	0.841	3.580
459	11:35:29	0.392	0.382	0.646	3.507
460	11:37:46	0.392	0.382	0.639	3.456
461	11:34:08	0.392	0.381	0.735	3.532
464	12:01:26	0.394	0.383	0.202	2.995
467	10:32:08	0.385	0.377	3.147	5.297
468	10:26:24	0.384	0.377	3.448	5.461
469	10:26:19	0.384	0.376	3.570	5.574
470	10:25:57	0.383	0.376	3.688	5.643
471	10:25:17	0.384	0.377	3.487	5.525
472	10:25:04	0.384	0.377	3.432	5.469
473	10:24:43	0.383	0.376	3.709	5.682
473	13:10:37	0.399	0.386	0.292	3.029
475	10:24:09	0.384	0.377	3.441	5.414
491	11:52:29	0.422	0.394	1.620	5.344
492	11:44:50	0.420	0.393	1.297	5.416
492	13:03:56	0.420	0.394	1.467	5.184
493	14:09:46	0.416	0.393	0.513	5.443
494	11:44:53	0.416	0.392	1.247	4.774
498	11:43:56	0.411	0.390	1.206	4.111
501	11:37:12	0.410	0.390	1.191	4.046
503	11:41:43	0.411	0.390	0.987	4.261
505	11:40:04	0.411	0.390	1.034	4.263
513	13:26:59	0.411	0.391	1.340	3.806
540	12:03:48	0.408	0.389	0.596	4.268
573	12:55:23	0.404	0.387	1.361	2.766

[a]Sol is the rover specific sol, LTST refers to the local true solar time, and x and y are the average chromaticities of the Sky Surveys. The chromaticity percent differences are calculated using the closest available Horizon Survey chromaticity values (by sol and time of day).

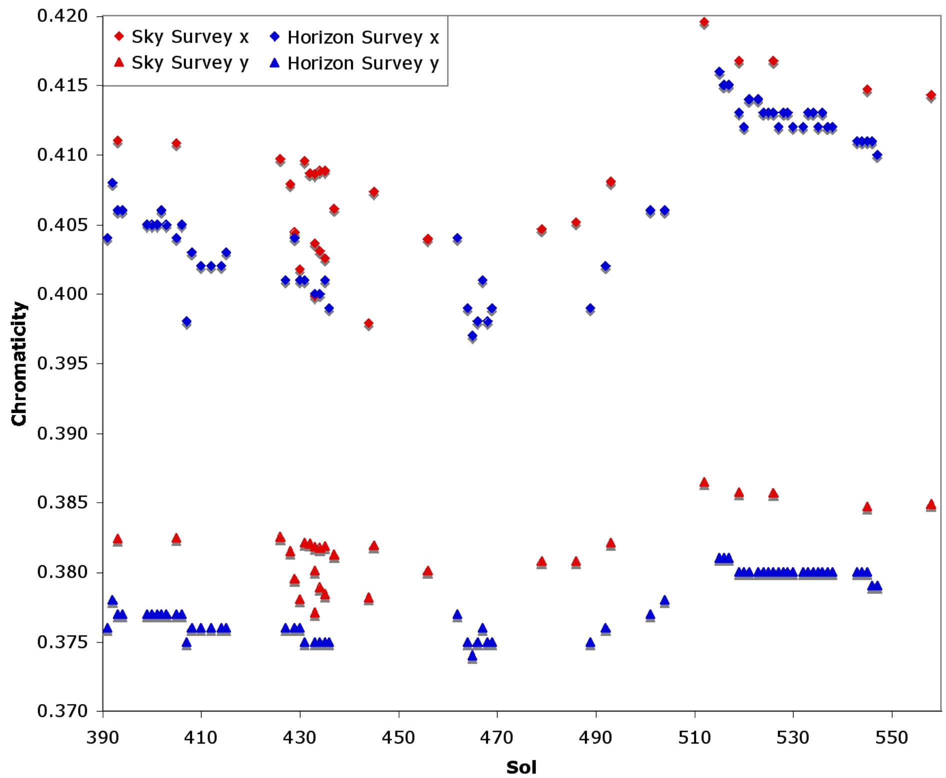

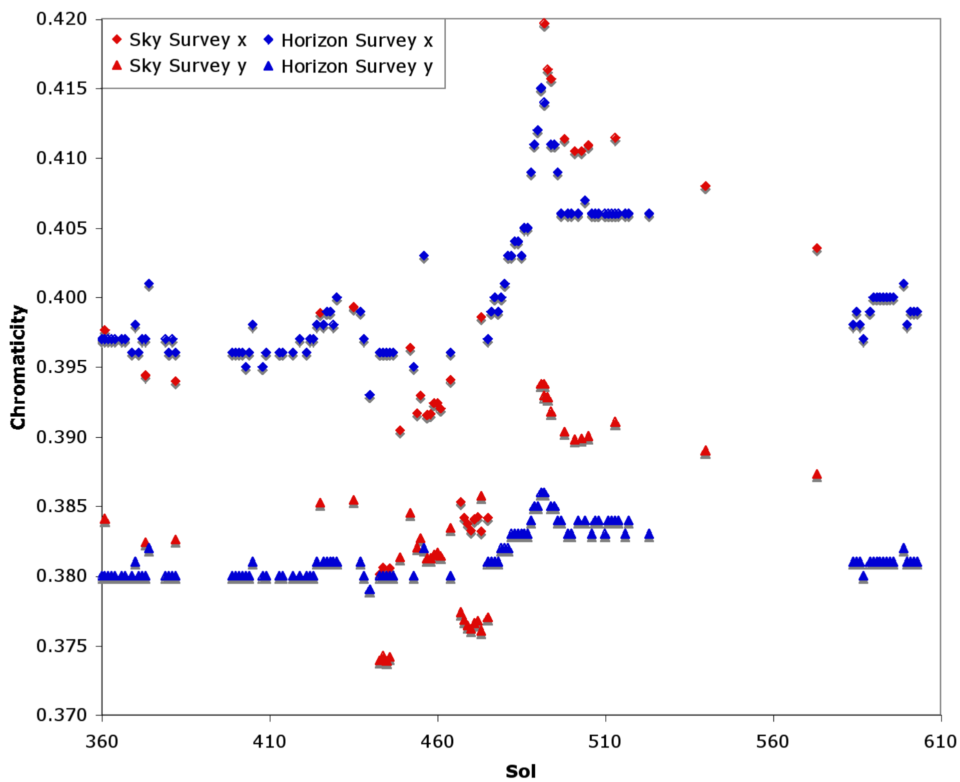

Figure 5. Chromaticities calculated from Pancam left eye 3 filter Horizon Surveys compared with those calculated from Pancam left eye 6 filter Sky Surveys. Data from Tables 1, 2, 3, and 4.

submitted manuscript, 2006]. These solar filters allow estimation of optical depth through direct extinction of sunlight. Similarly to the chromaticity values, systematic changes can be seen in optical depth values throughout the mission [*Lemmon et al.*, 2004; Lemmon et al., submitted manuscript, 2006]. The first 300 sols on both missions showed a trend that can be characterized as an exponential decay, followed by a series of sudden increases in optical

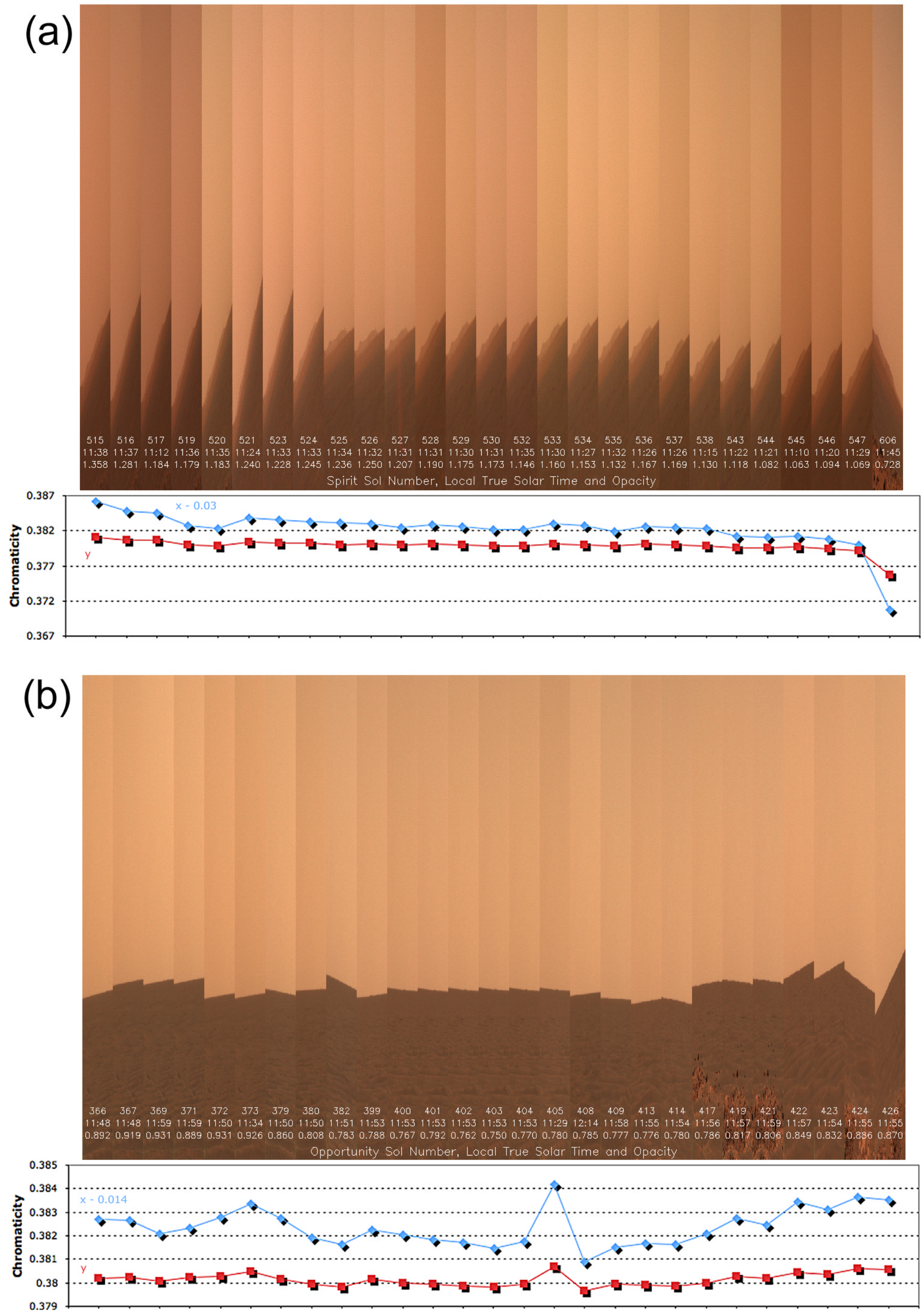

Figure 6

depth, each of which was followed by another decaying trend (Figure 8). These sharp increases and decay phases are very similar to those observed by Viking Lander 1 before and after the two major storms that it recorded [e.g., *Pollack et al.*, 1979].

[22] The sharp increases in optical depth begin after a solar longitude (L_s) of 120° and continue through L_s of about 300°. The season of greatest changes occurs during the northern fall, which is often associated with planet-wide storm activity [e.g., *Martin et al.*, 1992; *Martin and Zurek*, 1993; *Zurek and Martin*, 1993]. Increased solar heating, wind speed, and dust devil activity during this season place greater concentrations of dust particles into suspension in the atmosphere. This increases the optical depth, which then returns to its previous values as the dust settles out over weeks to month timescales [e.g., *Pollack et al.*, 1979; *Murphy et al.*, 1993].

[23] By comparing the measurements of optical depth and chromaticity, we can see that the changes in the two data sets correspond in time. For example, there is a sudden increase in both *x* and *y* sky chromaticity measured by Opportunity around sol 480, which peaks around

sol 491 (L_s of 228°). A smaller jump in chromaticity occurs around sol 430 (L_s of 190°). Both of these changes occur at exactly the same time as sudden increases in the optical depth. Similarly, the gradual decrease in x and y chromaticity seen in the Spirit data between sols 515 and 550 parallels the exponential decay of the optical depth values, which occurs after a sudden increase which peaks on sol 514.

7. Sky Color Compared to Soil Color

[24] The dust suspended in the Martian atmosphere absorbs sunlight, with the greatest absorption occurring between 400 to 600 nm [e.g., *Pollack et al.*, 1979; *Ockert-Bell et al.*, 1997]. The spectral properties of suspended atmospheric dust have long been known to be similar to those of ferric-rich high albedo regions and bright soil deposits [e.g., *McCord et al.*, 1977; *Bell*, 1992; *Clancy et al.*, 1995; *Bell et al.*, 2000, 2004a]. This has lead to the interpretation that many of the bright regions on Mars, from regional-scale high albedo features seen in telescopes down to small-scale bright wind ripples seen by landers and rovers, are the result of the settling and transport of a bright, globally homogeneous, and globally distributed aeolian dust unit [e.g., *Pollack and Sagan*, 1967; *Arvidson et al.*, 1989b; *Soderblom*, 1992]. Suspension of this dust in the atmosphere causes the visible color of the Martian sky as seen from the surface to be a strong function of the atmospheric dust loading.

[25] We can compare the sky chromaticities with those of the soil. Averaging chromaticity values for undisturbed, unshadowed soils in six images taken within 30 minutes of local noon between Opportunity sols 497 and 510 (Pancam sequences P2523, P2556, P2557, P2558, P2559, P2561), we calculate values of 0.434 for x and 0.394 for y. These values correspond to the ISCC-NBS color designation of "dark yellowish brown" as described by *Mundie* [1995]. The sky chromaticity never reaches this value, although both the x and y chromaticities were observed to increase linearly toward this point at various times during both rover missions. This is a strong indication that while the dust does not completely determine the color of the Martian sky, it provides a limiting value to the sky color in times of increased dust opacity.

[26] The qualitative similarities between trends in optical depth and chromaticity make it interesting to compare the two in more detail. When we plot chromaticity calculated from the Horizon Surveys as a function of optical depth calculated from the Pancam L8 solar filter data [*Lemmon et al.*, 2004; Lemmon et al., submitted manuscript, 2006], we see a definite functional relationship between the two (Figure 9). Second order polynomial fitting produces good-

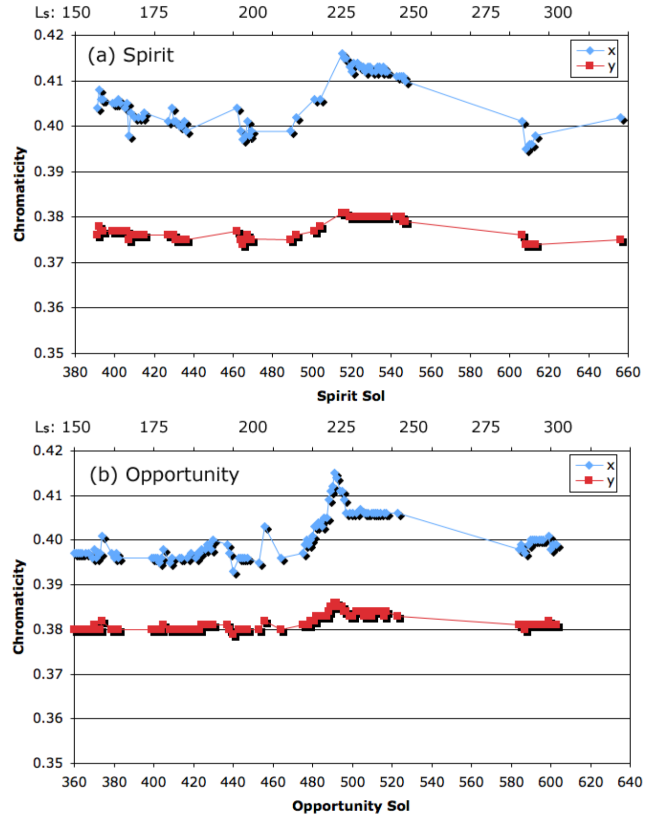

Figure 7. Chromaticities as a function of Sol for (a) Spirit data (except for sols 470 and 480) and (b) Opportunity data (Table 1). Chromaticities are calculated from L4, L5, and L6 filter data using equations (1) through (3). The x axes of these plots are offset by ~20 sols so that data points that are vertically aligned between the two rovers were acquired on the same Martian day.

Figure 6. (a) Martian sky color at the Spirit landing site as a function of time. These images were created by using the L4, L5, and L6 filters from the horizon surveys as the red, green, and blue inputs and scaling the entire group of resulting RGB images to their common minimum and maximum. The horizontal spatial axis has been compressed in each image by a large factor in order to display all of the sols shown on the same panel. These images are not intended to accurately represent the actual color of the scene, but provide a useful way to assess relative color changes with time. These Spirit Horizon Surveys were all taken within 30 minutes of 11:30 LTST. The sol, LTST, and average Pancam-derived L8 filter dust opacity for that sol (Lemmon et al., submitted manuscript, 2006) are listed in each panel. The lower plot shows the x (blue) and y (red) chromaticities derived for each of the Spirit Horizon Surveys (Table 1) shown in the top panel. The x values have been decreased by 0.03 chromaticity units just for ease of plotting both x and y on comparable scales. (b) Martian sky color at the Opportunity landing site as a function of time. Images compressed as described for Figure 6a. The panels shown here for Opportunity are a subset of the 88 sol Horizon Survey data set (Table 2), all taken within 30 minutes of 11:45 LTST. The sol, LTST, and average Pancam-derived L8 filter dust opacity for that sol (Lemmon et al., submitted manuscript, 2006) are listed in each panel. The lower plot shows the x (blue) and y (red) chromaticities derived for each of the Opportunity Horizon Surveys shown in the top panel. The x values have been decreased by 0.014 chromaticity units just for ease of plotting both x and y on comparable scales.

Table 5. Sky Chromaticity Measurements from the Viking Landers, Mars Pathfinder, and MERs[a]

	Viking 1	Viking 2	Pathfinder	Spirit	Opportunity
x	0.40	0.40	0.39–0.41	0.38–0.41	0.38–0.40
y	0.38	0.38	0.37–0.38	0.36–0.38	0.36–0.38

[a]Viking results are from *Huck et al.* [1977]; Pathfinder results are from *Maki et al.* [1999]. MER chromaticitiy values are averages of chromaticities calculated from sky flat images taken on sols 120, 280, and 377 for Spirit (sequences P2880, P2884, and P2886) and sols 4 and 353 for Opportunity (sequences P2701, P2867). These sky flats were shot at an elevation of 35°, using the cameras' automatic exposure algorithm and lossless compression [*Bell et al.*, 2006].

ness-of-fit coefficients on the order of 0.95 within the range of available data for the following functions:

$$\text{Spirit}: \left\{ \begin{aligned} x &= -0.0057\tau^2 + 0.0358\tau + 0.3781 \\ y &= -0.0004\tau^2 + 0.0102\tau + 0.3684 \end{aligned} \right\}$$
$$\text{Opportunity}: \left\{ \begin{aligned} x &= -0.0039\tau^2 + 0.0289\tau + 0.3756 \\ y &= -0.0022\tau^2 + 0.0118\tau + 0.3721 \end{aligned} \right\} \tag{4}$$

where x and y are the model fit chromaticities and τ is the daily average optical depth as measured through the Pancam L8 solar filter [*Lemmon et al.*, 2004; Lemmon et al., submitted manuscript, 2006].

8. Extrapolation to Zero Dust Opacity

[27] Our images and analyses allow us to provide an answer to a question that many people ask about the Martian sky: How would the sky color change as the dust opacity decreases, hypothetically all the way to zero dust? Extrapolation of our derived chromaticity-tau relationship outside the range of available data must obviously take into account the fact that the dust optical depth is not the only determinant of sky color on Mars. Specifically, Rayleigh scattering should become the most important source of sky color at some suitably low value of τ. Qualitatively, terrestrial experience would imply that the resulting low- or no-dust Martian sky would be blue. However, we have the capability to model this in a more quantitative fashion.

[28] We developed sky radiance models for a range of dust opacities to use as inputs to our chromaticity calculations described above. The models were computed using the multiple-scattering, discrete ordinates algorithm DISORT [*Stamnes et al.*, 1988]. We employed a 40 layer atmospheric model with 0.1 km resolution in the bottom 3 km of the atmosphere. The atmospheric density distribution was defined by solving the equation of hydrostatic equilibrium [cf. *Wolff and Clancy*, 2003] using a thermal profile from a MiniTES observation on Opportunity sol 440 at 12h30 local true solar time [e.g., *Smith et al.*, 2004]. The contribution of Rayleigh scattering was computed directly from the column density in each model layer. The dust vertical distribution was assumed to have a constant mixing ratio (dust number density to CO_2 number density) with altitude, with the single scattering albedo calculated for a canonical Martian polydispersion of spheres ($r_{eff} = 1.5\ \mu$m, $v_{eff} = 0.4$) using the indices of refraction of *Wolff and Clancy* [2003], which constrained the imaginary part using the Pathfinder analysis of *Tomasko et al.* [1999]. The dust phase function was adopted from *Clancy et al.* [2003] and assumed to be valid for all wavelengths. Finally, we specified a Lambert surface with the normal reflectance determined directly from the average Pancam surface radiance observations described in this paper.

[29] The model was applied for 6 Pancam band passes with the dust optical depth being tessellated with 50 points over the range [0,1]. We chose a scene geometry typical of the observations on Opportunity: solar incidence angle of 7.5°, an elevation angle of 10°, and an azimuth angle of 90° offset from that of the Sun. Although our model assumes a plane parallel atmosphere, comparison of such an air mass with that of a spherical atmosphere (i.e., a Chapman function with a 10 km scale height) shows differences of less than 10%. Finally, we required DISORT to employ 64 streams in order to adequately capture the angular dependence of the dust phase function [e.g., *Clancy et al.*, 2003].

[30] We can calculate chromaticity values from the DISORT model results in exactly the same fashion as for Pancam data. This produces a set of estimated chromaticities for the Martian sky for optical depth values which extend below the range of those measured by the rovers (Figure 10). The chromaticities derived from our DISORT model diverge dramatically from those derived from our empirical chromaticity versus optical depth model (Figure 9) at very low opacities. However, we can make direct comparisons at optical depth values measured by a rover. For example, at an optical depth of 0.75, the chromaticities calculated from the DISORT model results diverge from those calculated from Opportunity data by only about 6%. This gives us confidence that the DISORT model is generating reasonable estimates of typical Martian sky radiances as a function of opacity.

[31] Using the DISORT model results, we can predict the color change of the Martian sky if the optical depth were to fall to zero. We can extract information about color from the calculated chromaticities alone, scaling them to a common maximum and minimum as if they were pixels in one single image (Figure 11a). While this produces what we believe to be reasonably accurate absolute sky x and y estimates, it obviously does not provide a correct visual representation of what the Martian sky would look like. This is because the calculations that generated Figure 11a do not include an estimate of the sky's absolute brightness (luminance) at each value of optical depth.

[32] Because the method described for calculating the proper scaling factor for luminance depends on Pancam calibration data, there are multiple possible approaches to calculating the luminance values from the DISORT model radiance data. One possibility for calculating the actual luminance values for the model results is to use the scaling factor N derived above for use with Pancam data under similar lighting conditions. Since the DISORT model was set up to simulate the Horizon Survey sequences, it is logical to use the scaling factor calculated for these sequences when processing the model results. This yields luminance values which range from 0.167 to 0.0053 in the range of optical depths of 1.0 to 0.0. (Figure 11b). The brightest color shown here, corresponding to a dusty Martian atmosphere, is close to but slightly darker than what is referred to as "dark yellowish brown" in the NBS-ISCC color designation

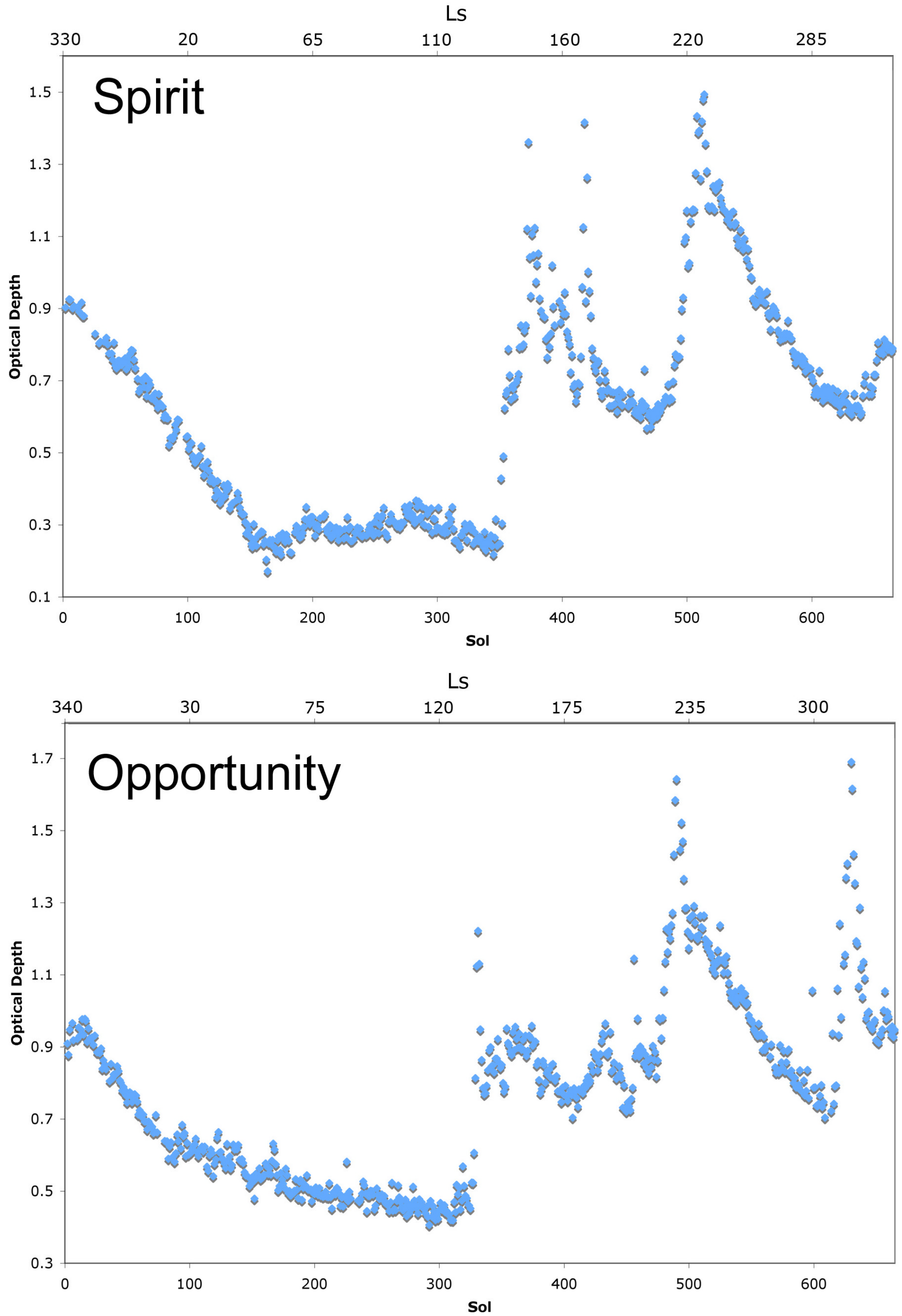

Figure 8. Optical depth as a function of sol and L_s for each rover. These values are averages of multiple daily optical depth measurements using the Pancam L8 filter [*Lemmon et al.*, 2004; Lemmon et al., submitted manuscript, 2006].

described by *Mundie* [1995]. The darkest color shown here, for τ = 0.0, lies between the NBS-ISCC designators of "bluish black" and "black".

[33] We can also estimate luminance values by calculating a scaling factor that would force the first point in the data set (optical depth of 1.0) to a specific luminance. Specifically, using the luminance (Y) value of 0.18 derived for the Martian sky by *Huck et al.* [1977] from Viking Lander data, we derive a luminance of 0.0057 at an optical depth of 0.0 (Figure 11c). Unfortunately, we cannot assess the accuracy of this scaling since *Huck et al.* [1977] did not report the value of τ that corresponded to their derived luminosity estimate. However, these derived colors are close to those derived in Figure 11b.

[34] Finally, we can scale the luminance directly on the basis of results from Pancam data. Since we know the optical depths for which each luminance value was calculated, we can select a more appropriate luminance value for

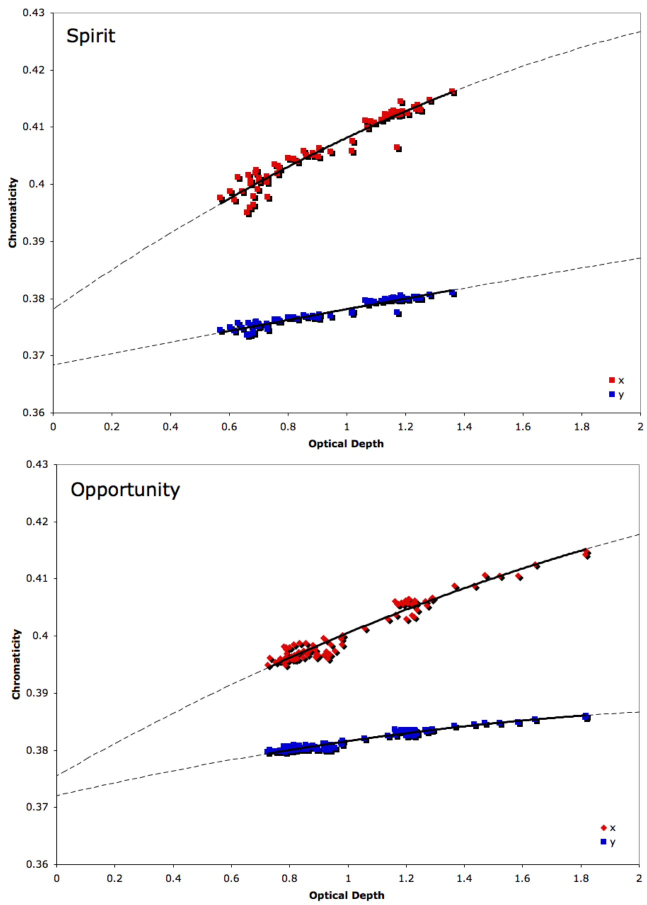

Figure 9. Chromaticity as a function of optical depth for each rover. Chromaticities are those used for Figure 7. Optical depth is a daily average (mostly consisting of near-noon values) as measured through the L8 filter (Figure 8).

scaling. For example, we find that the average luminance calculated from Horizon Surveys taken at optical depths of 1.0 is 0.173. Using this to scale the first point of the DISORT data set produces a luminance value of 0.0055 at an optical depth of 0.0 (Figure 11d). The results are very close to those derived for the alternate cases in Figures 11b and 11c. Apparently, although the luminance values change with different modeling approaches, these changes are too subtle to produce dramatic color differences to the human eye. This close agreement in the modeled perceived sky colors as a function of τ gives us confidence in the robustness of our results.

9. Implications for Future Mars Landed Missions

[35] We have demonstrated that there is an empirical relationship between sky chromaticity and measured optical depth, which, for optical depth values commonly encountered on Mars, provides the ability to approximate one of these values from the other. From an operational standpoint, this is currently not a particularly valuable correlation to exploit for the Mars Exploration Rovers. Estimating optical depth from sky chromaticity requires more rover resources (observing time, power, and data volume) than "normal" direct solar Beer's Law determination of τ [*Lemmon et al.*, 2004; Lemmon et al., submitted manuscript, 2006], which also serves as a way to determine and verify the rover's attitude and as input to daily models of rover solar panel power estimates. Going the other direction, calculating chromaticity from optical depth, would provide us with information about the current sky color and would save greatly in observation time and data volume, but would give us no detailed azimuthal or spectral information about the sky, both of which are known to vary significantly [e.g., *Pollack et al.*, 1979; *Tomasko et al.*, 1999; Lemmon et al., submitted manuscript, 2006].

[36] However, the situation could be different in the future for the rovers or other future missions. For example, the rover cameras mast azimuth or elevation actuators could fail in such a way that leaves the cameras able to take images, but not to point at the Sun. In that event, systematic opacity monitoring for science and power modeling purposes could be attempted using the relationship between optical depth and chromaticity that we have derived here. Alternately, future missions may be conducted that do not have (or which lose their capability for) direct solar imaging like that provided by the Mars Exploration Rover Pancam instruments. However, as long as they carry at least one camera capable of imaging the sky at visible wavelengths, opacities could be inferred and more general atmospheric studies and monitoring could be conducted.

[37] Finally, our conclusions as to the perceptual color of the Martian sky may have a significant impact on future human missions to Mars. Specifically, our results indicate that the predicted color of the Martian sky at zero optical depth can be described as something between bluish-black to black. A sky color differing so greatly from Earth's (from reddish to black) will undoubtedly add to the "alien" feel of the planet, and may even have unique psychological or physiological effects on astronauts. It is possible that if the sky ever got this dark, stars would be visible in the daytime, an experience noted by the Apollo astronauts during their

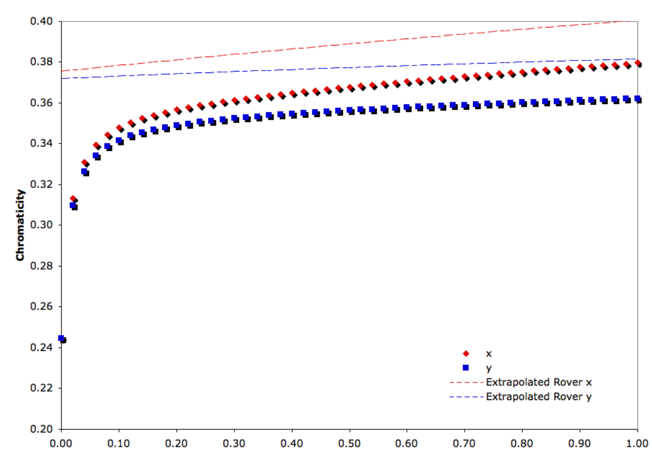

Figure 10. The data points represent chromaticities calculated from our DISORT model radiances of the Martian sky as a function of dust opacity. See text for model details. The dashed lines are the Opportunity chromaticity models of Figure 9 as a function of optical depth.

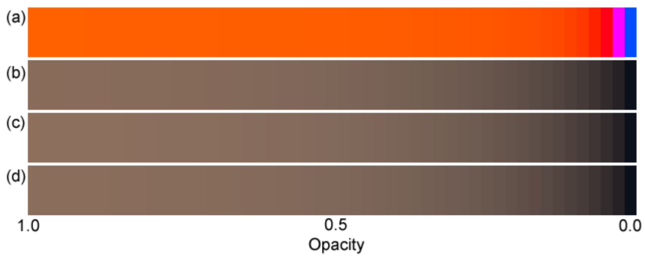

Figure 11. Color representations of DISORT model radiance values of the Martian sky for optical depths in 50 steps between 0.75 (left) to 0.0 (right). (a) Predicted sky chromaticities scaled to a common maximum and minimum with no dependence on luminance. These are predicted x and y values only and thus do not provide an accurate visual representation of how the sky color would be perceived by humans on Mars. (b) Predicted sky color including a scaling factor for luminance (Y) calculated for Pancam data taken in the same assumed conditions as our sky radiance model. (c) Predicted sky color again including luminances, but this time scaled to conform to a y value reported by *Huck et al.* [1977]. (d) Predicted sky color again including luminances, but this time scaled to conform to values calculated from Pancam average Horizon Survey data. See text for details.

exploration of the Moon's surface. The lowest dust opacity yet observed on Mars is around 0.2 (Figure 8 and Lemmon et al. (submitted manuscript, 2006)), a value which is just above what we would predict would be a strong decrease is brightness and "redness" of the sky at lower opacities. Does the opacity ever get low enough that the Martian sky would lose its distinctive reddish coloration? We will have to wait for future missions and future explorers to find out.

10. Conclusions

[38] We have developed a method for calculating chromaticity from Mars Exploration Rover Pancam data, enabling further quantitative studies of the colors of the Martian surface and sky. The numerical values derived for the sky chromaticities at the Spirit and Opportunity landing and traverse sites are consistent with those derived from Viking Lander and Mars Pathfinder sky imaging studies, and the MER data extend the range of observed sky chromaticity values as a function of dust opacity. Using systematic atmospheric sky color observations, we have been able to track systematic changes in the sky color over periods of several hundred sols. We have also found that these changes correlate with observed changes in measured optical depth, and have derived an empirical functional relationship between the chromaticity and opacity, allowing us to convert one set of values into the other with fairly high accuracy.

[39] Using a radiative transfer model of Martian sky radiances, we have demonstrated the inaccuracy of extrapolation of our derived functional relationship between chromaticity and opacity beyond the bounds of the optical depths observed so far in the MER missions. This model also allowed us to calculate the predicted change in sky color that would be seen if dust were completely removed from the Martian atmosphere and only Rayleigh scattering were responsible for generating sky color. Although the formally designated color of the sky would change from its typical "yellowish brown" to what is called "blue", the corresponding drop in luminance at low dust opacities would make the perceived sky color closer to what is called "bluish-black" or even "black," either way, much darker than the blue that we experience on Earth.

[40] **Acknowledgments.** We thank Jascha Sohl-Dickstein for assistance with the luminance scaling and other calculations described here and Mark Lemmon and the MER Atmospheric Sciences Theme Group members for assistance collecting and calculating the daily optical depth measurements from the rovers. We also thank the Mars Exploration Rover operations and science teams and the Pancam engineering and test teams for making these observations, and all the others from these amazing roving vehicles, possible. This work is supported by grants from the Mars Exploration Rover Project at JPL to Cornell University.

References

Arvidson, R. E., E. A. Guinness, H. J. Moore, J. Tillman, and S. D. Wall (1983), Three Mars Years: Viking Lander 1 Imaging Observations, *Science*, *222*, 463–468.
Arvidson, R. E., J. L. Gooding, and H. J. Moore (1989a), The Martian surface as imaged, sampled, and analyzed by the Viking Landers, *Rev. Geophys.*, *27*, 39–60.
Arvidson, R. E., E. A. Guinness, M. A. Dale-Bannister, J. B. Adams, M. O. Smith, P. R. Christensen, and R. B. Singer (1989b), Nature and distribution of surficial deposits in Chryse Planitia and vicinity, Mars, *J. Geophys. Res.*, *94*, 1573–1587.
Arvidson, R. E., et al. (2006), Overview of the Spirit Mars Exploration Rover Mission to Gusev Crater: Landing site to Backstay Rock in the Columbia Hills, *J. Geophys. Res.*, *111*, E02S01, doi:10.1029/2005JE002499.
Bell, J. F., III (1992), Charge-coupled device imaging spectroscopy of Mars. 2. Results and implications for Martian ferric mineralogy, *Icarus*, *100*, 575–597.
Bell, J. F., III, et al. (2000), Mineralogic and compositional properties of Martian soil and dust: Results from Mars Pathfinder, *J. Geophys. Res.*, *105*, 1721–1755.
Bell, J. F., III, et al. (2003), Mars Exploration Rover Athena Panoramic Camera (Pancam) investigation, *J. Geophys. Res.*, *108*(E12), 8063, doi:10.1029/2003JE002070.
Bell, J. F., III, et al. (2004a), Pancam multispectral imaging results from the Spirit rover at Gusev crater, *Science*, *305*, 800–806.
Bell, J. F., III, et al. (2004b), Pancam multispectral imaging results from the Opportunity rover at Meridiani Planum, *Science*, *306*, 1703–1709.
Bell, J. F., III, J. Joseph, J. N. Sohl-Dickstein, H. M. Arneson, M. J. Johnson, M. T. Lemmon, and D. Savransky (2006), In-flight calibration and performance of the Mars Exploration Rover Panoramic Camera (Pancam) instruments, *J. Geophys. Res.*, *111*, E02S03, doi:10.1029/2005JE002444.
Clancy, R. T., S. W. Lee, G. R. Gladstone, W. W. McMillan, and T. Roush (1995), A new model for Mars atmospheric dust based upon analysis of ultraviolet through infrared observations from Mariner 9, Viking, and Phobos, *J. Geophys. Res.*, *100*, 5251–5264.
Clancy, R. T., M. J. Wolff, and P. R. Christensen (2003), Mars aerosol studies with the MGS TES emission phase function observations: Optical depths, particle sizes, and ice cloud types versus latitude and solar longitude, *J. Geophys. Res.*, *108*(E9), 5098, doi:10.1029/2003JE002058.
Commission Internationale de l'Eclairage (CIE) (1932), *Commission Internationale de l'Eclairage Proceedings, 1931*, Cambridge Univ. Press, New York.
Huck, F. O., D. J. Jobson, S. K. Park, S. D. Wall, R. E. Arvidson, W. R. Patterson, and W. D. Benton (1977), Spectrophotometric and color estimates of the Viking Lander sites, *J. Geophys. Res.*, *82*(28), 440–441.
Kelly, K. L., and D. B. Judd (1976), *Color: Universal Language and Dictionary of Names*, *Spec. Publ. 440*, U.S. Natl. Bur. of Standards, Washington, D. C.
Lemmon, M. T., et al. (2004), Atmospheric imaging results from the Mars Exploration Rovers: Spirit and Opportunity, *Science*, *306*, 1753–1756.
Maki, J. N., J. J. Lorre, P. H. Smith, R. D. Brandt, and D. J. Steinwand (1999), The color of Mars: Spectrophotometric measurements at the Pathfinder landing site, *J. Geophys. Res.*, *104*(E4), 8781–8794.
Martin, L. J., and R. W. Zurek (1993), An analysis of the history of dust activity on Mars, *J. Geophys. Res.*, *98*, 3221–3246.

Martin, L. J., P. B. James, A. Dollfus, K. Iwasaki, and J. D. Beish (1992), Telescopic observations: Visual, photographic, polarimetric, in *Mars*, edited by H. H. Kieffer et al., pp. 34–70, Univ. of Ariz. Press, Tucson.
McCord, T. B., R. L. Huguenin, D. Mink, and C. Pieters (1977), Spectral reflectance of Martian areas during the 1973 opposition: Photoelectric filter photometry, 0.33–1.10 μm, *Icarus*, *31*, 25–39.
Mundie, D. A. (1995), The NBS/ISCC Color System, Polymath Syst., Pittsburgh, Pa. (Available at http://www.anthus.com/Colors/NBS.html)
Murphy, J. R., R. M. Haberle, O. B. Toon, and J. B. Pollack (1993), Martian global dust storms: Zonally symmetric numerical simulations including size-dependent particle transport, *J. Geophys. Res.*, *98*, 3197–3220.
Ockert-Bell, M. E., J. F. Bell III, C. P. McKay, J. B. Pollack, and F. Forget (1997), Absorption and scattering properties of the Martian dust in the solar wavelengths, *J. Geophys. Res.*, *102*, 9039–9050.
Pollack, J. B., and C. Sagan (1967), Secular changes and dark-area regeneration on Mars, *Icarus*, *6*, 434–439.
Pollack, J. B., D. S. Colburn, F. M. Flaser, R. Kahn, C. E. Carlston, and D. Pidek (1979), Properties and effects of dust particles suspended in the Martian atmosphere, *J. Geophys. Res.*, *84*, 2929–2945.
Shepard, M. K. (2001), The Bloomsburg University Goniometer (B. U. G.) Laboratory: An integrated laboratory for measuring bidirectional reflectance functions, *Lunar Planet. Sci.* [CD-ROM], *XXXII*, Abstract 1015.
Smith, M. D., et al. (2004), First atmospheric science results from the Mars Exploration Rovers Mini-TES, *Science*, *306*(5702), 1750–1753.
Soderblom, L. A. (1992), The composition and mineralogy of the Martian surface from spectroscopic observations: 0.3–50 μm, in *Mars*, edited by H. H. Kieffer et al., pp. 557–593, Univ. of Ariz. Press, Tucson.
Stamnes, K., S. C. Tsay, W. Wiscombe, and K. Jayaweera (1988), Numerically stable algorithm for discrete ordinate method radiative transfer in multiple scattering and emitting layered media, *Appl. Opt.*, *27*, 2502–2509.
Tomasko, M. G., L. R. Doose, M. Lemmon, P. H. Smith, and E. Wegryn (1999), Properties of dust in the Martian atmosphere from the Imager on Mars Pathfinder, *J. Geophys. Res.*, *104*, 8987–9008.
Wolff, M. J., and R. T. Clancy (2003), Constraints on the size of Martian aerosols from Thermal Emission Spectrometer observations, *J. Geophys. Res.*, *108*(E9), 5097, doi:10.1029/2003JE002057.
Wolff, M. J., S. W. Lee, R. T. Clancy, L. J. Martin, P. B. James, and J. F. Bell III (1997), Observations of dust storms on Mars with the Hubble Space Telescope, *J. Geophys. Res.*, *102*, 1679–1692.
Wyszecki, G., and W. S. Stiles (1982), *Color Science: Concepts and Methods, Quantitative Data and Formulae*, 2nd ed., John Wiley, Hoboken, N. J.
Zurek, R. W., and L. J. Martin (1993), Interannual variability of planet-encircling dust storms on Mars, *J. Geophys. Res.*, *98*, 3247–3259.

J. F. Bell III and D. Savransky, Department of Astronomy, Cornell University, 402 Space Sciences Building, Ithaca, NY 14853-6801, USA. (jfb8@cornell.edu)
M. J. Wolff, Space Science Institute, Boulder, CO 80309, USA.